Dimensionality effects in the local density of states of ferromagnetic hosts probed via STM: Spin-polarized quantum beats and spin filtering

A. C. Seridonio,[1,2] S. C. Leandro,[1] L. H. Guessi,[1] E. C. Siqueira,[1] F. M. Souza,[3] E. Vernek,[3] M. S. Figueira,[4] and J. C. Egues[5]

[1]*Departamento de Física e Química, Universidade Estadual Paulista, Ilha Solteira, São Paulo 15385-000, Brazil*

[2]*Departamento de Física, Instituto de Geociências e Ciências Exatas-IGCE, Universidade Estadual Paulista, Rio Claro, São Paulo 13506-970, Brazil*

[3]*Instituto de Física, Universidade Federal de Uberlândia, Uberlândia, Minais Gerais 38400-902, Brazil*

[4]*Instituto de Física, Universidade Federal Fluminense, Niterói, Rio de Janeiro 24210-340, Brazil*

[5]*Instituto de Física de São Carlos, Universidade de São Paulo, São Carlos, São Paulo 13560-970, Brazil*

(Received 15 November 2012; published 5 March 2013)

We theoretically investigate the local density of states (LDOS) probed by an STM tip of ferromagnetic metals hosting a single adatom and a subsurface impurity. We model the system via the two-impurity Anderson Hamiltonian. By using the equation of motion with the relevant Green's functions, we derive analytical expressions for the LDOS of two host types: a surface and a quantum wire. The LDOS reveals Friedel-like oscillations and Fano interference as a function of the STM tip position. These oscillations strongly depend on the host dimension. Interestingly, we find that the spin-dependent Fermi wave numbers of the hosts give rise to spin-polarized *quantum beats* in the LDOS. Although the LDOS for the metallic surface shows a damped beating pattern, it exhibits the opposite behavior in the quantum wire. Due to this absence of damping, the wire operates as a spatially resolved spin filter with a high efficiency.

DOI: 10.1103/PhysRevB.87.125104 PACS number(s): 07.79.Fc, 74.55.+v, 85.75.−d, 72.25.−b

I. INTRODUCTION

The local density of states (LDOS) of electronic systems with impurities can exhibit Fano line shapes due to the quantum interference between different electron paths. Such interference arises from the itinerant electrons that travel through the host and tunnel into the impurity sites.[1,2] For a single magnetic adatom in the Kondo regime[3] probed by a scanning tunneling microscope (STM) tip, interesting features manifest when one has a spin-polarized electron bath present. Here, we mention the splitting of the Kondo peak in the differential conductance due to the itinerant magnetism of the host.[4] Such a hallmark has already been found experimentally in an Fe island with a Co adatom.[5] Additionally, the STM system can also operate as a Fano-Kondo spin filter due to a spin-polarized tip and a nonmagnetic host.[6,7] In the absence of a ferromagnetic host, the Fano-Kondo profile becomes doubly degenerate.[8–23] Away from the Kondo regime, a spin diode emerges.[24]

In the condensed-matter literature on scanning microscopy, there is a profusion of work discussing spin-dependent phenomena employing ferromagnetic leads coupled to quantum dots or adatoms in the Kondo regime.[4,6,7,25–44] Here, we mention those with metallic samples and buried impurities in which the anisotropy of the Fermi surface plays an important role in electron tunneling.[45–50] According to the experiment of Prüser *et al.*,[45] such anisotropy allows atoms of Fe and Co beneath the Cu(100) surface to scatter electrons in preferential directions of the material due to an effect called "electron focusing." In this scenario, the STM becomes a new tool for the detection of the Fermi surface signatures in the real lattice of a metal. In contrast, much less attention has been devoted to spin-polarized systems away from the Kondo regime[51–53] and with two impurities.

Thus, in this paper, we present a theoretical description of the systems sketched in Fig. 1. We show that interesting phenomena, such as the spin-polarized quantum beats in the LDOS and the spin-filtering effect, arise. To this end, we consider two distinct geometries consistent with recent experiments: a metallic surface and a quantum wire. The two-dimensional (2D) case emulates the Fe island in Ref. 5. The quantum wire on the other hand, mimics the electron-focusing effect investigated in Ref. 45. Interestingly, we note that the pioneering quantum wire treatment for electron focusing in a side-coupled geometry can be found in Ref. 49. In this treatment, the noninteracting single-impurity Anderson model[54] was solved in one dimension (1D) by considering the impurity above the wire. We should also point out that the full *ab initio* calculation that yields to electron focusing in Ref. 45

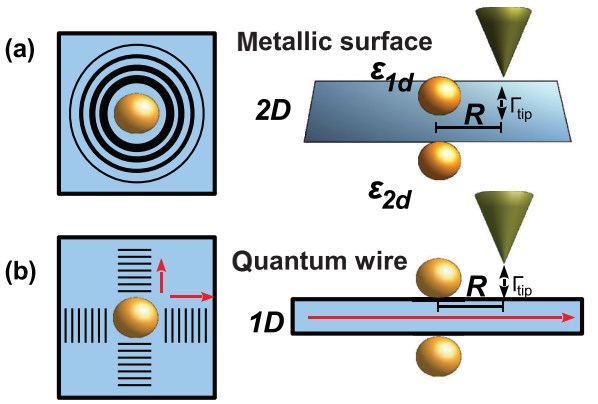

FIG. 1. (Color online) Side-coupled geometry with two impurities in the presence of an STM tip. $\Gamma_{tip} = \pi w^2 \rho_{tip}$, where w and ρ_{tip} are the tip-host hopping term and the DOS for the STM probe, respectively. (a) Left panel: 2D evanescent waves appear in the LDOS of a metallic surface. The system is treated as a two-dimensional electron gas shown in the right panel. (b) Left panel: the confinement of 1D waves in specific directions (perpendicular wave fronts) is due to the electron-focusing effect (see Ref. 45). Each direction is modeled by a quantum wire as illustrated in the right panel.

can be qualitatively recovered by the simple quantum wire model adopted in Ref. 49.

Here, we extend this one-dimensional treatment of the Anderson Hamiltonian by including a spin-dependent DOS for the wire, a second lateral impurity right beneath it, and Coulomb interaction in both impurities. We perform our study in the framework of the two-impurity Anderson model by employing the equation-of-motion approach to calculate the LDOS of the system. The Hubbard I approximation[55] is used by assuming, for the sake of simplicity, infinite Coulomb energies at the impurities. We show that the LDOS can be written in terms of the Fano factor, the Friedel-like function for charge oscillations, and the spin-dependent Fermi wave numbers of the host. Such quantities lead to spin-polarized quantum beats in the LDOS. We also show that this effect is strongly correlated to the host dimensionality. Thus, the quantum beats in the LDOS of the metallic surface present a long-range damped behavior in contrast to the undamped one found in the quantum wire system. Such distinct features originate from the specific forms assumed by the Fano factor and Friedel function, which depend on the dimensionality of the host. Therefore, the metallic surface and the quantum wire become spatially resolved spin filters where the latter displays a higher efficiency due to the undamped LDOS.

This paper is organized as follows. In Sec. II, we show the theoretical model of the ferromagnetic hosts with the impurities in the side-coupled geometry as sketched in Fig. 1 and derive the LDOS formula for both systems, the metallic surface, and the quantum wire. The decoupling scheme Hubbard I[55] for the Green's functions is presented in Sec. III. In Sec. IV, we discuss the results for the quantum beats in the LDOS and the spin filtering. The conclusions appear in Sec. V.

II. THEORETICAL MODEL

A. Hamiltonian

In order to probe the LDOS of the ferromagnetic hosts, we represent an STM tip weakly connected to hosts hybridized to a pair of side-coupled impurities as outlined in Fig. 1. The systems we investigate are described according to the two-impurity Anderson model given by the Hamiltonian,[3]

$$\mathcal{H} = \sum_{\vec{k}\sigma} \varepsilon_{\vec{k}\sigma} c^{\dagger}_{\vec{k}\sigma} c_{\vec{k}\sigma} + \sum_{j\sigma} \varepsilon_{jd} d^{\dagger}_{j\sigma} d_{j\sigma} + \sum_{j} U_j d^{\dagger}_{j\uparrow} d_{j\uparrow} d^{\dagger}_{j\downarrow} d_{j\downarrow} + \sum_{j\vec{k}\sigma} \left[\frac{V_{j\vec{k}}}{\sqrt{\mathcal{N}}} \phi^{*}_{\vec{k}}(\vec{R}_j) c^{\dagger}_{\vec{k}\sigma} d_{j\sigma} + \frac{V^{*}_{j\vec{k}}}{\sqrt{\mathcal{N}}} \phi_{\vec{k}}(\vec{R}_j) d^{\dagger}_{j\sigma} c_{\vec{k}\sigma} \right]. \tag{1}$$

The spin-polarized electron gas forming the hosts is described by the operator $c^{\dagger}_{\vec{k}\sigma}$ ($c_{\vec{k}\sigma}$) for the creation (annihilation) of an electron in a quantum state labeled by the wave vector $\vec{k}$, spin σ, and energy $\varepsilon_{\vec{k}\sigma}$. For the impurities, $d^{\dagger}_{j\sigma}$ ($d_{j\sigma}$) creates (annihilates) an electron with spin σ in state ε_{jd} with $j = 1,2$. The third term of Eq. (1) accounts for the on-site Coulomb interaction U_j at the jth impurity placed at position $\vec{R}_j$. In our calculations, we assume $U_1 = U_2 \to \infty$ for the sake of simplicity.[56] Finally, the last two terms mix the host continuum of states and the levels ε_{jd}. This hybridization occurs at the impurity sites $\vec{R}_j$ via the host-impurity couplings $V_{j\vec{k}}$ and the plane waves $\phi_{\vec{k}}(\vec{R}_j) = e^{i\vec{k}\cdot\vec{R}_j}$. $\mathcal{N}$ is the number of conduction states. The ferromagnetic hosts are considered spin-polarized electron baths, characterized by the polarization,

$$P = \frac{\rho_{FM\uparrow} - \rho_{FM\downarrow}}{\rho_{FM\uparrow} + \rho_{FM\downarrow}}, \tag{2}$$

in which

$$\rho_{FM\sigma} = \rho_0(1 + \sigma P) \tag{3}$$

is the density of states of the hosts at the chemical potential in a Stoner-like framework,[57,58] expressed in terms of the density ρ_0 for the case $P = 0$.

B. LDOS for the spin-polarized systems

To obtain the host LDOS, we introduce the retarded Green's function in the time coordinate,

$$\mathcal{G}_{\sigma}(t,\vec{R}) = -\frac{i}{\hbar}\theta(t)\mathcal{Z}^{-1}_{FM} \sum_{n} e^{-\beta E_n} \langle n|[\tilde{\Psi}_{\sigma}(\vec{R},t)\tilde{\Psi}^{\dagger}_{\sigma}(\vec{R},0)]_{+}|n\rangle, \tag{4}$$

where

$$\tilde{\Psi}_{\sigma}(\vec{R}) = \frac{1}{\sqrt{\mathcal{N}}} \sum_{\vec{k}} \phi_{\vec{k}}(\vec{R}) c_{\vec{k}\sigma} \tag{5}$$

is the fermionic operator describing the quantum state of the host site placed below the STM tip, $\hbar$ is the Planck constant divided by 2π, $\theta(t)$ is the step function at the instant t, $\beta = 1/k_B T$ with k_B as the Boltzmann constant and T as the system temperature, $\mathcal{Z}_{FM}$ and $|n\rangle$ are the partition function and a many-body eigenstate of the system Hamiltonian [Eq. (1)], respectively, and $[\cdots,\cdots]_{+}$ is the anticommutator for Eq. (5) evaluated at distinct times. From Eq. (4), the spin-dependent LDOS at a site $\vec{R}$ of the host [see Fig. 1] can be obtained as

$$\rho^{\sigma}_{\mathrm{LDOS}}(\varepsilon,R) = -\frac{1}{\pi}\mathrm{Im}\{\tilde{\mathcal{G}}_{\sigma}(\varepsilon^{+},\vec{R})\}, \tag{6}$$

where $\tilde{\mathcal{G}}_{\sigma}(\varepsilon^{+},\vec{R})$ is the time Fourier transform of $\mathcal{G}_{\sigma}(t,\vec{R})$. Here, $\varepsilon^{+} = \varepsilon + i\eta$ and $\eta \to 0^{+}$. In what follows, we first develop a general formalism for impurities localized at arbitrary positions $\vec{R}_j$ and $\vec{R}_l$; later on, we take the limit $\vec{R}_j = \vec{R}_l = \vec{0}$ in order to treat the side-coupled geometry of this paper.

To obtain an analytical expression for the LDOS, we apply the equation-of-motion approach to Eq. (4). Thus, we substitute Eq. (5) in Eq. (4) and begin the procedure with

$$\mathcal{G}_{\sigma}(t,\vec{R}) = \frac{1}{\mathcal{N}} \sum_{\vec{k}\vec{q}} \phi_{\vec{k}}(\vec{R})\phi^{*}_{\vec{q}}(\vec{R})\mathcal{G}^{\sigma}_{c_{\vec{k}}c_{\vec{q}}}(t) \tag{7}$$

expressed in terms of

$$\mathcal{G}^{\sigma}_{c_{\vec{k}}c_{\vec{q}}}(t) = -\frac{i}{\hbar}\theta(t)\mathcal{Z}^{-1}_{FM} \sum_{n} e^{-\beta E_n} \langle n|[c_{\vec{k}\sigma}(t), c^{\dagger}_{\vec{q}\sigma}(0)]_{+}|n\rangle. \tag{8}$$

Performing $\frac{\partial}{\partial t}$ on Eq. (8), we find

$$\frac{\partial}{\partial t}\mathcal{G}^{\sigma}_{c_{\vec{k}}c_{\vec{q}}}(t) = -\frac{i}{\hbar}\delta(t)\mathcal{Z}^{-1}_{FM}\sum_{n} e^{-\beta E_n}\langle n|[c_{\vec{k}\sigma}(t),c^{\dagger}_{\vec{q}\sigma}(0)]_{+}|n\rangle + \left(-\frac{i}{\hbar}\right)\varepsilon_{\vec{k}\sigma}\mathcal{G}^{\sigma}_{c_{\vec{k}}c_{\vec{q}}}(t) + \left(-\frac{i}{\hbar}\right) \times \frac{1}{\sqrt{\mathcal{N}}}\sum_{j} V_{j\vec{k}}\phi^{*}_{\vec{k}}(\vec{R}_j)\mathcal{G}^{\sigma}_{d_j c_{\vec{q}}}(t), \tag{9}$$

where we have used

$$i\hbar\frac{\partial}{\partial t}c_{\vec{k}\sigma}(t) = [c_{\vec{k}\sigma},\mathcal{H}] = \varepsilon_{\vec{k}\sigma}c_{\vec{k}\sigma}(t) + \frac{1}{\sqrt{\mathcal{N}}}\sum_{j} V_{j\vec{k}}\phi^{*}_{\vec{k}}(\vec{R}_j)d_{j\sigma}(t). \tag{10}$$

In the energy coordinate, we solve Eq. (9) for $\tilde{\mathcal{G}}^{\sigma}_{c_{\vec{k}}c_{\vec{q}}}(\varepsilon^{+})$ and obtain

$$\tilde{\mathcal{G}}^{\sigma}_{c_{\vec{k}}c_{\vec{q}}}(\varepsilon^{+}) = \frac{\delta_{\vec{k}\vec{q}}}{\varepsilon^{+}-\varepsilon_{\vec{k}\sigma}} + \frac{1}{\sqrt{\mathcal{N}}}\sum_{j}\frac{V_{j\vec{k}}\phi^{*}_{\vec{k}}(\vec{R}_j)}{\varepsilon^{+}-\varepsilon_{\vec{k}\sigma}}\tilde{\mathcal{G}}^{\sigma}_{d_j c_{\vec{q}}}(\varepsilon^{+}). \tag{11}$$

Notice that we need to find the mixed Green's function $\tilde{\mathcal{G}}^{\sigma}_{d_j c_{\vec{q}}}(\varepsilon^{+})$. To this end, we define the advanced Green's function,

$$\mathcal{F}^{\sigma}_{d_j c_{\vec{q}}}(t) = \frac{i}{\hbar}\theta(-t)\mathcal{Z}^{-1}_{FM}\sum_{n} e^{-\beta E_n}\langle n|[d^{\dagger}_{j\sigma}(0),c_{\vec{q}\sigma}(t)]_{+}|n\rangle, \tag{12}$$

which results in

$$\frac{\partial}{\partial t}\mathcal{F}^{\sigma}_{d_j c_{\vec{q}}}(tt) = -\frac{i}{\hbar}\delta(t)\mathcal{Z}^{-1}_{FM}\sum_{n} e^{-\beta E_n} \times \langle n|[d^{\dagger}_{j\sigma}(0),c_{\vec{q}\sigma}(t)]_{+}|n\rangle - \frac{i}{\hbar}\varepsilon_{\vec{q}\sigma}\mathcal{F}^{\sigma}_{d_j c_{\vec{q}}}(t) + \left(-\frac{i}{\hbar}\right)\frac{1}{\sqrt{\mathcal{N}}}\sum_{l} V_{l\vec{q}}\phi^{*}_{\vec{q}}(\vec{R}_l)\mathcal{F}^{\sigma}_{d_j d_l}(t), \tag{13}$$

where, once again, we used Eq. (10), interchanging $\vec{k}\leftrightarrow\vec{q}$. Thus, the Fourier transform of Eq. (13) becomes

$$\varepsilon^{-}\tilde{\mathcal{F}}^{\sigma}_{d_j c_{\vec{q}}}(\varepsilon^{-}) = \varepsilon_{\vec{q}\sigma}\tilde{\mathcal{F}}^{\sigma}_{d_j c_{\vec{q}}}(\varepsilon^{-}) + \frac{1}{\sqrt{\mathcal{N}}}\sum_{l} V_{l\vec{q}}\phi^{*}_{\vec{q}}(\vec{R}_l)\tilde{\mathcal{F}}^{\sigma}_{d_j d_l}(\varepsilon^{-}), \tag{14}$$

with $\varepsilon^{-} = \varepsilon - i\eta$. Applying the property,

$$\tilde{\mathcal{G}}^{\sigma}_{d_j c_{\vec{q}}}(\varepsilon^{+}) = \left\{\tilde{\mathcal{F}}^{\sigma}_{d_j c_{\vec{q}}}(\varepsilon^{-})\right\}^{\dagger} \tag{15}$$

to Eq. (14), we show that

$$\varepsilon^{+}\tilde{\mathcal{G}}^{\sigma}_{d_j c_{\vec{q}}}(\varepsilon^{+}t) = \varepsilon_{\vec{q}\sigma}\tilde{\mathcal{G}}^{\sigma}_{d_j c_{\vec{q}}}(\varepsilon^{+}) + \frac{1}{\sqrt{\mathcal{N}}}\sum_{l} V^{*}_{l\vec{q}}\phi_{\vec{q}}(\vec{R}_l)\tilde{\mathcal{G}}^{\sigma}_{d_j d_l}(\varepsilon^{+}), \tag{16}$$

and

$$\tilde{\mathcal{G}}^{\sigma}_{d_j c_{\vec{q}}}(\varepsilon^{+}) = \frac{1}{\sqrt{\mathcal{N}}}\sum_{l}\frac{V^{*}_{l\vec{q}}\phi_{\vec{q}}(\vec{R}_l)}{\varepsilon^{+}-\varepsilon_{\vec{q}\sigma}}\tilde{\mathcal{G}}^{\sigma}_{d_j d_l}(\varepsilon^{+}). \tag{17}$$

Now, we substitute Eq. (17) into Eq. (11) and the latter into Eq. (7) in the energy coordinate to obtain

$$\tilde{\mathcal{G}}_{\sigma}(\varepsilon^{+},R) = \frac{1}{\mathcal{N}}\sum_{\vec{k}}\frac{|\phi_{\vec{k}}(\vec{R})|^2}{\varepsilon^{+}-\varepsilon_{\vec{k}\sigma}} + (\pi\rho_0)^2\sum_{j}(q_{j\sigma}-iA_{j\sigma})(q_j-iA_{j\sigma})\tilde{\mathcal{G}}^{\sigma}_{d_j d_j}(\varepsilon) + (\pi\rho_0)^2\sum_{j\neq l}(q_{j\sigma}-iA_{j\sigma})(q_{l\sigma}-iA_{l\sigma})\tilde{\mathcal{G}}^{\sigma}_{d_j d_l}(\varepsilon). \tag{18}$$

It is worth mentioning that the imaginary part of the first term of Eq. (18) gives the background DOS of the host [Eq. (3)] and the others describe impurity contributions with

$$q_{j\sigma} = \frac{1}{\pi\rho_0\mathcal{N}}\sum_{\vec{k}}\frac{V_{j\vec{k}}\phi^{*}_{\vec{k}}(\vec{R}_j)\phi_{\vec{k}}(\vec{R})}{\varepsilon-\varepsilon_{\vec{k}\sigma}} \tag{19}$$

being the Fano parameter due to the single coupling $V_{j\vec{k}}$ between the host and a given impurity. This factor encodes the quantum interference originated by electrons traveling through the ferromagnetic conduction band that tunnel to the impurity state and return to the band and those that do not perform such trajectories. The definition of Eq. (19) is in accordance with Fano's theory[1,2] and leads to interference patterns in the LDOS as we see in Sec. IV. Additionally, we recognize

$$A_{j\sigma} = \frac{1}{\rho_0\mathcal{N}}\sum_{\vec{k}} V_{j\vec{k}}\phi^{*}_{\vec{k}}(\vec{R}_j)\phi_{\vec{k}}(\vec{R})\delta(\varepsilon-\varepsilon_{\vec{k}\sigma}) = |A_{j\sigma}|e^{i\alpha_{j\sigma}} \tag{20}$$

as an expression that we call the Friedel function because it leads to Friedel-like oscillations in the LDOS with $\alpha_{j\sigma}$ as a spin-dependent phase. In the end, the Green's function $\tilde{\mathcal{G}}_{\sigma}(\varepsilon^{+},R)$, indeed, depends on $\tilde{\mathcal{G}}^{\sigma}_{d_j d_j}(\varepsilon)$ and the mixed Green's function $\tilde{\mathcal{G}}^{\sigma}_{d_j d_l}(\varepsilon)$. Finally, from Eqs. (6) and (18), the LDOS of the ferromagnetic systems can be recast as the expression,

$$\rho^{\sigma}_{\mathrm{LDOS}}(\varepsilon,R) = \rho_{FM\sigma} + \pi\rho_0^2\sum_{j}\Big[\left(|A_{j\sigma}|^2-q^2_{j\sigma}\right)\mathrm{Im}\{\tilde{\mathcal{G}}^{\sigma}_{d_j d_j}(\varepsilon)\} + 2q_{j\sigma}|A_{j\sigma}|\sin\left(\alpha_{j\sigma}+\frac{\pi}{2}\right)\mathrm{Re}\{\tilde{\mathcal{G}}^{\sigma}_{d_j d_j}(\varepsilon)\}\Big] + \pi\rho_0^2\sum_{j\neq l}\Delta\varrho_{jl\sigma}, \tag{21}$$

where

$$\Delta\varrho_{jl\sigma} = -q_{j\sigma}q_{l\sigma}\mathrm{Im}\{\tilde{\mathcal{G}}^{\sigma}_{d_j d_l}(\varepsilon)\} + \Big[|A_{j\sigma}|q_{l\sigma}\cos\left(\alpha_{j\sigma}+\frac{\pi}{2}\right) + |A_{j\sigma}||A_{l\sigma}|\cos(\alpha_{j\sigma}-\alpha_{l\sigma}) - q_{j\sigma}|A_{l\sigma}|\cos\left(\alpha_{l\sigma}+\frac{\pi}{2}\right)\Big]\mathrm{Im}\{\tilde{\mathcal{G}}^{\sigma}_{d_j d_l}(\varepsilon)\} + \Big[q_{j\sigma}|A_{l\sigma}|\sin\left(\alpha_{l\sigma}+\frac{\pi}{2}\right) + q_{l\sigma}|A_{j\sigma}| \times \sin\left(\alpha_{j\sigma}+\frac{\pi}{2}\right) + |A_j||A_l|\sin(\alpha_{j\sigma}-\alpha_{l\sigma})\Big] \times \mathrm{Re}\{\tilde{\mathcal{G}}^{\sigma}_{d_j d_l}(\varepsilon)\}. \tag{22}$$

The set of Eqs. (21) and (22) is the main analytical finding of this paper. It describes the spin-dependent LDOS in ferromagnetic hosts with two impurities localized at distinct sites $\vec{R}_j$. In the absence of the last term of Eq. (21), it reduces to the case of two decoupled systems with one impurity each. The terms in Eq. (22), indeed, hybridize such single-impurity problems via the mixed Green's functions $\tilde{\mathcal{G}}^{\sigma}_{d_j d_l}(\varepsilon)$. Thus, the LDOS formula encodes the single Fano factor $q_{j\sigma}$, the Friedel-like function $A_{j\sigma}$, and the new interfering term $\Delta\varrho_{jl\sigma}$.

We close this section by recalling that phase $\alpha_{j\sigma}$ is nonzero for the quantum wire system as we will see later. The quantities $q_{j\sigma}$ and $A_{j\sigma}$ in the quantum wire device are, indeed, functions that exhibit undamped oscillations as the tip moves away from the impurities. Conversely, damped oscillations are predicted in the metallic surface setup. In this case, $\alpha_{j\sigma} = 0$, and $A_{j\sigma}$ becomes a real function. Thus, the quantity $|A_{j\sigma}|$ should be read just as $A_{j\sigma}$ in Eqs. (21) and (22). Moreover, a ferromagnetic environment is characterized by two spin-dependent Fermi wave numbers, namely, $k_{F\uparrow}$ and $k_{F\downarrow}$, which, at low polarization P, introduce a slight difference between them. As a result, this feature leads to a full LDOS $\rho^{\uparrow}_{\mathrm{LDOS}} + \rho^{\downarrow}_{\mathrm{LDOS}}$ with spin-polarized quantum beats that can be damped or undamped depending upon the system dimensionality.[59] We will look more closely at these features later.

In STM experiments, in particular, within the linear-response regime and neglecting tip-adatom coupling, the differential conductance $G = G^{\uparrow} + G^{\downarrow}$ is the observable measured by the tip, whose spin component is given by[4]

$$G^{\sigma} = \frac{e^2}{h}\pi\Gamma_{\mathrm{tip}}\int_{-\infty}^{+\infty}\rho^{\sigma}_{\mathrm{LDOS}}(\varepsilon)\left[-\frac{\partial f}{\partial\varepsilon}(\varepsilon-\phi)\right]d\varepsilon, \tag{23}$$

where e is the electron charge ($e > 0$), $\Gamma_{\mathrm{tip}} = \pi w^2\rho_{\mathrm{tip}}$ is the tip-host coupling expressed in terms of the hopping term w and the DOS ρ_{tip} for the STM probe, f is the Fermi-Dirac distribution, and ϕ is the applied bias. For $\phi < 0$, the host is the source of electrons, and the tip is the drain. For $\phi > 0$, we have the opposite. It is useful to define the dimensionless LDOS,

$$LDOS = \frac{\rho^{\uparrow}_{\mathrm{LDOS}} + \rho^{\downarrow}_{\mathrm{LDOS}}}{\rho_{FM\uparrow} + \rho_{FM\downarrow}} \tag{24}$$

and the transport polarization,

$$P_T = \frac{G^{\uparrow} - G^{\downarrow}}{G^{\uparrow} + G^{\downarrow}}, \tag{25}$$

in order to investigate the spin-polarized quantum beats as we see in Sec. IV. Recall that, in the absence of the impurities, the transport polarization of Eq. (25) becomes $P_T = P$ for low enough temperatures as established by Eq. (2). In Sec. IV, we verify that Eq. (25) oscillates around P, exhibiting two distinct behaviors as a result of the system dimensionality—damped spin-polarized quantum beats in the metallic surface setup and an undamped pattern in the quantum wire device.

C. Fano and Friedel-like functions for the metallic surface system

In this section, we calculate the expressions for the Fano parameter [Eq. (19)] and the Friedel-like function [Eq. (20)] in the metallic surface case where no manifestation of electron focusing occurs. This calculation was previously performed in the single-impurity problem,[4] and now we present an extension applied to the double-impurity system. We begin by taking into account the linear dispersion relation,

$$\varepsilon_{k\sigma} = k^{-1}_{F\sigma}D_{\sigma}(k - k_{F\sigma}), \tag{26}$$

which depends on the expression,

$$k_{F\downarrow} = \sqrt{\frac{1-P}{1+P}}k_{F\uparrow} \tag{27}$$

determined from Eq. (3) and on the bottom band $D_{\sigma} = D + \sigma\Delta$ with D as the unpolarized half-width and Δ as the Stoner splitting.[35] In particular, for a small polarization P, Eq. (27) results in slightly different Fermi wave numbers and, consequently, in spin-polarized quantum beats in the full LDOS as we will see.

In order to solve Eq. (20), we assume $\phi_{\vec{k}}(\vec{R}) = e^{ikR\cos\theta_k}$ for the electronic 2D wave function and use

$$J_0(\xi) = \frac{1}{2\pi}\int_0^{2\pi} e^{i\xi\cos\theta_k}d\theta_k, \tag{28}$$

the angular representation for the zeroth-order Bessel function. Thus, in the wideband limit $|\varepsilon| \ll D_{\sigma}$ with the flat-band DOS,

$$\rho_{FM\sigma} = \frac{\mathcal{S}}{\mathcal{N}2\pi}\left\{k\left(\frac{d\varepsilon_{k\sigma}}{dk}\right)^{-1}\right\}_{k=k_{F\sigma}} \tag{29}$$

expressed in terms of the spin-dependent Fermi wave number $k_{F\sigma}$, the periodicity area $\mathcal{S}$ in the host, and by using $V_{j\vec{k}} = V$, we find

$$A_{j\sigma} = \frac{\rho_{FM\sigma}}{\rho_0}V J_0(k_{F\sigma}\tilde{R}) \equiv A^{2D}_{j\sigma} \tag{30}$$

for the Friedel-like function with $\tilde{R} = |\vec{R} - \vec{R}_j|$ as the relative coordinate of the STM tip with respect to the jth impurity. Notice that, according to Eq. (20), phase $\alpha_{j\sigma}$ is zero and Eq. (30) is a real quantity. In the case of the Fano parameter, we start defining the advanced Green's function,

$$\bar{\mathcal{G}}_{j\sigma} = \frac{1}{\mathcal{N}}\sum_{\vec{k}}\frac{V_{j\vec{k}}\phi^{*}_{\vec{k}}(\vec{R}_j)\phi_{\vec{k}}(\vec{R})}{\varepsilon - \varepsilon_{\vec{k}\sigma} - i\eta}, \tag{31}$$

by assuming the spin and energy dependencies in the Lorentzian shape,

$$V_{j\vec{k}\sigma} = V\frac{\Delta^2}{\Delta^2 + \varepsilon^2_{k\sigma}}, \tag{32}$$

in order to obtain an analytical solution for $q_{j\sigma}$ via a regularization procedure.[4] Later on, we take the limit $\Delta \gg |\varepsilon_{k\sigma}|$ to show that Eq. (32) recovers the case $V_{j\vec{k}\sigma} = V$. Thus, we can write the identities,

$$q_{j\sigma} = \frac{1}{\pi\rho_0}\mathrm{Re}\{\bar{\mathcal{G}}_{j\sigma}\} \equiv q^{2D}_{j\sigma}, \tag{33}$$

and

$$A^{2D}_{j\sigma} = \frac{1}{\pi\rho_0}\mathrm{Im}\{\bar{\mathcal{G}}_{j\sigma}\}, \tag{34}$$

which allow us to close the calculation. Equations (33) and (34) imply the relation,

$$q_{j\sigma}^{2D} = \frac{1}{\pi\rho_0}\bar{\mathcal{G}}_{j\sigma} - iA_{j\sigma}^{2D}. \tag{35}$$

As the Friedel function is already known from Eq. (30), the quantity $\frac{1}{\pi\rho_0}\bar{\mathcal{G}}_{j\sigma}(\varepsilon,R)$ provides a relationship for the Fano parameter. To this end, we can write

$$\frac{1}{\pi\rho_0}\bar{\mathcal{G}}_{j\sigma} = \frac{1}{2}\frac{\rho_{FM\sigma}}{\rho_0}V\sum_{l=1}^{2}\bar{\mathcal{G}}_{jl\sigma}, \tag{36}$$

with $\bar{\mathcal{G}}_{jl\sigma}(\varepsilon,R)$ obeying the following integral representation:

$$\bar{\mathcal{G}}_{jl\sigma} = \frac{1}{\pi}\int_{-\infty}^{+\infty} d\varepsilon_{k\sigma}\frac{\Delta^2}{\Delta^2+\varepsilon_{k\sigma}^2}\frac{1}{\varepsilon-\varepsilon_{k\sigma}-i\eta}H_0^{(l)}(k\tilde{R}). \tag{37}$$

In the equation above, we have used, for the sake of simplicity, Eq. (26) and the Hankel functions $H_0^{(1)}(\xi) = J_0(\xi) + iY_0(\xi)$ and $H_0^{(2)}(\xi) = J_0(\xi) - iY_0(\xi)$. Looking at Eq. (37), we calculate the integral $\bar{\mathcal{G}}_{j1\sigma}$ by choosing a counterclockwise contour over a semicircle in the upper half of the complex plane, which includes the simple pole $\varepsilon_{k\sigma} = +i\Delta$. Applying the residue theorem, we obtain

$$\bar{\mathcal{G}}_{j1\sigma} = H_0^{(1)}(k_\Delta\tilde{R})\frac{\Delta}{\varepsilon-i\Delta}, \tag{38}$$

with $k_\Delta = k_{F\sigma}(1+i\frac{\Delta}{D_\sigma})$. For the evaluation of $\bar{\mathcal{G}}_{j2\sigma}$, we used a clockwise contour over a semicircle in the lower-half plane, including the poles $\varepsilon_{k\sigma} = \varepsilon - i\eta$ and $\varepsilon_{k\sigma} = -i\Delta$, which yields

$$\bar{\mathcal{G}}_{j2\sigma} = 2iH_0^{(2)}(k_\varepsilon\tilde{R})\frac{\Delta^2}{\Delta^2+\varepsilon^2} + \frac{\Delta}{\varepsilon+i\Delta}H_0^{(2)}(k_\Delta^*\tilde{R}), \tag{39}$$

with $k_\varepsilon = k_{F\sigma}(1+\frac{\varepsilon}{D_\sigma})$. Taking the property $H_0^{(2)}(\xi) = [H_0^{(1)}(\xi^*)]^*$ for the second term in Eq. (39) into account, Eq. (36) becomes

$$\frac{1}{\pi\rho_0}\bar{\mathcal{G}}_{j\sigma} = \frac{\rho_{FM\sigma}}{\rho_0}V\left[iH_0^{(2)}(k_\varepsilon\tilde{R})\frac{\Delta^2}{\Delta^2+\varepsilon^2} + \mathrm{Re}\left\{H_0^{(1)}(k_\Delta\tilde{R})\frac{\Delta}{\varepsilon-i\Delta}\right\}\right]. \tag{40}$$

Explicit calculation of the terms in the brackets of Eq. (40) leads to

$$iH_0^{(2)}(k_\varepsilon\tilde{R})\frac{\Delta^2}{\Delta^2+\varepsilon^2} = iJ_0(k_{F\sigma}\tilde{R}) + Y_0(k_{F\sigma}\tilde{R}) \tag{41}$$

and

$$\mathrm{Re}\left\{H_0^{(1)}(k_\Delta\tilde{R})\frac{\Delta}{\varepsilon-i\Delta}\right\} = -Y_0(k_{F\sigma}\tilde{R}), \tag{42}$$

where we have assumed $|\varepsilon| \ll D_\sigma$, $\Delta \ll D_\sigma$, and $\Delta \gg |\varepsilon|$. In order to ensure the limit $V_{j\vec{k}} = V$ in Eq. (32), we perform the substitution of Eqs. (30), (40), (41), and (42) in Eq. (35), showing that

$$q_{j\sigma}^{2D} = 0 \tag{43}$$

for any value of $k_{F\sigma}\tilde{R}$.

To summarize, the zero value of the Fano parameter given by Eq. (43) and the zeroth-order Bessel function $J_0(k_{F\sigma}\tilde{R})$ found in Eq. (30) lead to long-range damped spin-polarized quantum beats in the full LDOS. This feature is discussed in Sec. IV.

D. Fano and Friedel-like functions for the quantum wire system

Here, we determine the Fano parameter in Eq. (19) and the Friedel-like function in Eq. (20) for the quantum wire case. Following Weismann,[49] we use $\phi_{\vec{k}}(\vec{R}) = e^{ikR}$ as the electron wave function in which the direction introduced by $\vec{R}$ defines the STM tip-impurity distance where electron focusing manifests. We also use the dispersion relation,

$$\varepsilon_{k\sigma} = \frac{\hbar^2k^2}{2m} - D_\sigma \tag{44}$$

measured with respect to the bottom band D_σ and the flat DOS,

$$\rho_{FM\sigma} = \frac{\mathcal{L}}{\mathcal{N}2\pi}\left(\frac{d\varepsilon_{k\sigma}}{dk}\right)^{-1}_{k=k_{F\sigma}} = \frac{\mathcal{L}}{\mathcal{N}2\pi}\frac{m}{\hbar^2k_{F\sigma}}, \tag{45}$$

with m as the effective electron mass and $\mathcal{L}$ as the length of periodicity in the wire. Additionally, in the wideband limit $|\varepsilon| \ll D_\sigma$, we find the following complex Friedel-like function:

$$A_{j\sigma} = V\frac{\rho_{FM\sigma}}{\rho_0}e^{ik_{F\sigma}\tilde{R}} \equiv A_{j\sigma}^{1D} \tag{46}$$

characterized by a spin-dependent phase $\alpha_{j\sigma} = k_{F\sigma}\tilde{R}$. This phase results in undamped oscillatory behavior as a function of $\tilde{R} = |\vec{R} - \vec{R}_j|$, which also appears in $q_{j\sigma}^{1D}$. Thus, we take Eqs. (44) and (45) into account rewriting Eq. (19) as

$$q_{j\sigma} = \frac{V}{\pi\rho_0\mathcal{N}}\sum_{\vec{k}}\frac{e^{ik\tilde{R}}}{\varepsilon-\varepsilon_k} = 2V\frac{\mathcal{L}}{\rho_0\mathcal{N}\pi}\frac{m}{\hbar^2}\mathcal{I} \equiv q_{j\sigma}^{1D}, \tag{47}$$

with

$$\mathcal{I} = -\frac{1}{2\pi}\mathrm{P}\int_{-\infty}^{+\infty}\frac{e^{ik\tilde{R}}}{k^2-k_\varepsilon^2}dk = \frac{\sin(k_{F\sigma}\tilde{R})}{2k_{F\sigma}}, \tag{48}$$

in the limit $|\varepsilon| \ll D_\sigma$ and with P as the principal value. Finally, we obtain the Fano factor,

$$q_{j\sigma}^{1D} = 2V\frac{\rho_{FM\sigma}}{\rho_0}\sin(k_{F\sigma}\tilde{R}), \tag{49}$$

which also presents spin-dependent Fermi wave numbers $k_{F\uparrow}$ and $k_{F\downarrow}$ as in Eq. (46). Here, they are still connected via Eq. (27), thus, leading to undamped spin-polarized quantum beats in the full LDOS.

III. CALCULATION OF THE IMPURITY GREEN'S FUNCTION

In the present section, we calculate $\tilde{\mathcal{G}}_{d_jd_l}^{\sigma}(\varepsilon)$ $(j,l = 1,2)$ that appear in Eqs. (21) and (22) for the LDOS. To handle the interacting term of the Hamiltonian, we adopt the Hubbard I approximation,[55] which provides reliable results at temperatures above the Kondo temperature.[55] We begin by repeating the equation-of-motion approach for these Green's functions,

which results in

$$(\varepsilon - \tilde{\varepsilon}_{jd\sigma} + i\Gamma_{jj\sigma})\tilde{\mathcal{G}}^{\sigma}_{d_j d_j} = 1 + U_j \tilde{\mathcal{G}}_{d_{j\sigma} n_{d_{j\bar{\sigma}}}, d_{j\sigma}} + \left(\Sigma^R_{ljj\sigma} - i\Gamma_{lj\sigma}\right)\tilde{\mathcal{G}}^{\sigma}_{d_l d_j}, \quad (50)$$

and

$$(\varepsilon - \tilde{\varepsilon}_{ld\sigma} + i\Gamma_{ll\sigma})\tilde{\mathcal{G}}^{\sigma}_{d_l d_j} = U_l \tilde{\mathcal{G}}_{d_{l\sigma} n_{d_{l\bar{\sigma}}}, d_{j\sigma}} + \left(\Sigma^R_{jj\sigma} - i\Gamma_{jj\sigma}\right)\tilde{\mathcal{G}}^{\sigma}_{d_j d_j}, \quad (51)$$

where $\tilde{\varepsilon}_{jd\sigma} = \varepsilon_{jd} + \Sigma^R_{jj\sigma}$ for $l \neq j$. In the equation above, $\tilde{\mathcal{G}}_{d_{l\sigma} n_{d_{l\bar{\sigma}}}, d_{j\sigma}}$ is a higher-order Green's function obtained from the time Fourier transform of

$$\mathcal{G}_{d_{l\sigma} n_{d_{l\bar{\sigma}}}, d_{j\sigma}}(t) = -\frac{i}{\hbar}\theta(t)\mathcal{Z}^{-1}_{FM} \times \sum_n e^{-\beta E_n}\langle n|[d_{l\sigma}(t) n_{d_{l\bar{\sigma}}}(t), d^{\dagger}_{j\sigma}(0)]_+|n\rangle, \quad (52)$$

with $n_{d_{l\bar{\sigma}}} = d^{\dagger}_{l\bar{\sigma}} d_{l\bar{\sigma}}$ being the number operator of the lth impurity with spin $\bar{\sigma}$ (opposite to σ). Here,

$$\Sigma^R_{lj\sigma} = \frac{1}{\mathcal{N}} \sum_{\vec{k}} \frac{V^*_{j\vec{k}} V_{l\vec{k}} \phi_{\vec{k}}(\vec{R}_j)\phi^*_{\vec{k}}(\vec{R}_l)}{\varepsilon - \varepsilon_{\vec{k}\sigma}} \quad (53)$$

represents the real part of the noninteracting self-energy $\Sigma_{lj\sigma}$ and

$$\Sigma^I_{lj\sigma} = -\Gamma_{lj\sigma} = -\frac{1}{\mathcal{N}}\pi \sum_{\vec{k}} V^*_{j\vec{k}} V_{l\vec{k}} \phi_{\vec{k}}(\vec{R}_j)\phi^*_{\vec{k}}(\vec{R}_l)\delta(\varepsilon - \varepsilon_{\vec{k}\sigma}) \quad (54)$$

describes the corresponding imaginary part, which plays the role of a generalized Anderson parameter $\Gamma_{lj\sigma}$. In order to close the system of Green's functions in Eqs. (50) and (51), we first take the time derivative of Eq. (52) and then perform the time Fourier transform. With that, we obtain

$$\begin{aligned}(\varepsilon^+ - \varepsilon_{ld} - U_l)\tilde{\mathcal{G}}_{d_{l\sigma} n_{d_{l\bar{\sigma}}}, d_{j\sigma}} &= \delta_{lj}\langle n_{d_{l\bar{\sigma}}}\rangle + \left(-\sum_{\vec{k}} \frac{1}{\sqrt{\mathcal{N}}} V_{l\vec{k}} \phi^*_{\vec{k}}(\vec{R}_l)\right)\tilde{\mathcal{G}}_{c^{\dagger}_{\vec{k}\bar{\sigma}} d_{l\bar{\sigma}} d_{l\sigma}, d_{j\sigma}} \\ &+ \left(\sum_{\vec{k}} \frac{1}{\sqrt{\mathcal{N}}} V^*_{l\vec{k}} \phi_{\vec{k}}(\vec{R}_l)\right)\tilde{\mathcal{G}}_{c_{\vec{k}\sigma} d^{\dagger}_{l\bar{\sigma}} d_{l\bar{\sigma}}, d_{j\sigma}} \\ &+ \left(\sum_{\vec{k}} \frac{1}{\sqrt{\mathcal{N}}} V^*_{l\vec{k}} \phi_{\vec{k}}(\vec{R}_l)\right)\tilde{\mathcal{G}}_{d^{\dagger}_{l\bar{\sigma}} c_{\vec{k}\bar{\sigma}} d_{l\sigma}, d_{j\sigma}}, \end{aligned} \quad (55)$$

which also depends on new Green's functions on the same order of $\tilde{\mathcal{G}}_{d_{l\sigma} n_{d_{l\bar{\sigma}}}, d_{j\sigma}}$ and on the average occupation number $\langle n_{d_{l\bar{\sigma}}}\rangle$, that is, calculated as

$$\langle n_{d_{l\bar{\sigma}}}\rangle = \int_{-\infty}^{+\infty} d\varepsilon \left\{-\frac{1}{\pi}\mathrm{Im}(\tilde{\mathcal{G}}^{\bar{\sigma}}_{d_l d_l})\right\} f(\varepsilon). \quad (56)$$

Within the Hubbard I approximation, we truncate the Green's functions $\tilde{\mathcal{G}}_{c^{\dagger}_{\vec{k}\bar{\sigma}} d_{l\bar{\sigma}} d_{l\sigma}, d_{j\sigma}}$ and $\tilde{\mathcal{G}}_{d^{\dagger}_{l\bar{\sigma}} c_{\vec{k}\bar{\sigma}} d_{l\sigma}, d_{j\sigma}}$ according to the decoupling scheme,

$$\tilde{\mathcal{G}}_{c^{\dagger}_{\vec{k}\bar{\sigma}} d_{l\bar{\sigma}} d_{l\sigma}, d_{j\sigma}} \simeq \langle c^{\dagger}_{\vec{k}\bar{\sigma}} d_{l\bar{\sigma}}\rangle \tilde{\mathcal{G}}^{\sigma}_{d_l d_j}, \quad (57)$$

$$\tilde{\mathcal{G}}_{d^{\dagger}_{l\bar{\sigma}} c_{\vec{k}\bar{\sigma}} d_{l\sigma}, d_{j\sigma}} \simeq \langle c^{\dagger}_{\vec{k}\bar{\sigma}} d_{l\bar{\sigma}}\rangle \tilde{\mathcal{G}}^{\sigma}_{d_l d_j}, \quad (58)$$

and apply the equation-of-motion approach to $\tilde{\mathcal{G}}_{c_{\vec{k}\sigma} d^{\dagger}_{l\bar{\sigma}} d_{l\bar{\sigma}}, d_{j\sigma}}$. In order to cancel the second term with the last one in Eq. (55), we simultaneously combine the approximations in Eqs. (57) and (58) with the property,

$$\sum_{\vec{k}} \frac{1}{\sqrt{\mathcal{N}}} V_{l\vec{k}} \phi^*_{\vec{k}}(\vec{R}_l) = \sum_{\vec{k}} \frac{1}{\sqrt{\mathcal{N}}} V^*_{l\vec{k}} \phi_{\vec{k}}(\vec{R}_l), \quad (59)$$

which is only fulfilled on a metallic surface system, whereas, for the quantum wire, it holds in the side-coupled geometry $\vec{R}_l = \vec{R}_j = \vec{0}$. Bearing this in mind, we can rewrite Eq. (55) as follows:

$$(\varepsilon - \varepsilon_{ld} - U_l + i\eta)\tilde{\mathcal{G}}_{d_{l\sigma} n_{d_{l\bar{\sigma}}}, d_{j\sigma}} = \delta_{lj}\langle n_{d_{l\bar{\sigma}}}\rangle + \left(\sum_{\vec{k}} \frac{1}{\sqrt{\mathcal{N}}} V^*_{l\vec{k}} \phi_{\vec{k}}(\vec{R}_l)\right)\tilde{\mathcal{G}}_{c_{\vec{k}\sigma} d^{\dagger}_{l\bar{\sigma}} d_{l\bar{\sigma}}, d_{j\sigma}}. \quad (60)$$

Once again, employing the equation-of-motion approach for $\tilde{\mathcal{G}}_{c_{\vec{k}\sigma} d^{\dagger}_{l\bar{\sigma}} d_{l\bar{\sigma}}, d_{j\sigma}}$, we find

$$\begin{aligned}(\varepsilon^+ - \varepsilon_{\vec{k}\sigma})\tilde{\mathcal{G}}_{c_{\vec{k}\sigma} d^{\dagger}_{l\bar{\sigma}} d_{l\bar{\sigma}}, d_{j\sigma}} &= V_{l\vec{k}} \frac{1}{\sqrt{\mathcal{N}}} \phi^*_{\vec{k}}(\vec{R}_l)\tilde{\mathcal{G}}_{d_l n_{d_{l\bar{\sigma}}}, d_{j\sigma}} \\ &+ \sum_{\vec{q}} V^*_{l\vec{q}} \frac{1}{\sqrt{\mathcal{N}}} \phi_{\vec{q}}(\vec{R}_l)\tilde{\mathcal{G}}_{c_{\vec{k}\sigma} d^{\dagger}_{l\bar{\sigma}} c_{\vec{q}\bar{\sigma}}, d_{j\sigma}} \\ &- \sum_{\vec{q}} V_{l\vec{q}} \frac{1}{\sqrt{\mathcal{N}}} \phi^*_{\vec{q}}(\vec{R}_l)\tilde{\mathcal{G}}_{c^{\dagger}_{\vec{q}\bar{\sigma}} d_{l\bar{\sigma}} c_{\vec{k}\sigma}, d_{j\sigma}} \\ &+ \sum_{\vec{j}\neq l} V_{\vec{j}\vec{k}} \frac{1}{\sqrt{\mathcal{N}}} \phi^*_{\vec{k}}(\vec{R}_{\vec{j}})\tilde{\mathcal{G}}_{d_{\vec{j}} n_{d_{l\bar{\sigma}}}, d_{j\sigma}}. \end{aligned} \quad (61)$$

Here, we continue with the Hubbard I scheme, proceeding as in Eqs. (57) and (58) by making the following approximations:

$$\tilde{\mathcal{G}}_{c_{\vec{k}\sigma} d^{\dagger}_{l\bar{\sigma}} c_{\vec{q}\bar{\sigma}}, d_{j\sigma}} \simeq \langle d^{\dagger}_{l\bar{\sigma}} c_{\vec{q}\bar{\sigma}}\rangle \tilde{\mathcal{G}}_{c_{\vec{k}\sigma} d_{j\sigma}}, \quad (62)$$

$$\tilde{\mathcal{G}}_{c^{\dagger}_{\vec{q}\bar{\sigma}} d_{l\bar{\sigma}} c_{\vec{k}\sigma}, d_{j\sigma}} \simeq \langle d^{\dagger}_{l\bar{\sigma}} c_{\vec{q}\bar{\sigma}}\rangle \tilde{\mathcal{G}}_{c_{\vec{k}\sigma} d_{j\sigma}}, \quad (63)$$

$$\tilde{\mathcal{G}}_{d_{\vec{j}\sigma} n_{d_{l\bar{\sigma}}}, d_{j\sigma}} \simeq \langle n_{d_{l\bar{\sigma}}}\rangle \tilde{\mathcal{G}}^{\sigma}_{d_{\vec{j}} d_j}, \quad (64)$$

and replacing Eq. (59) in Eq. (61) to show that

$$\tilde{\mathcal{G}}_{c_{\vec{k}\sigma} d^{\dagger}_{l\bar{\sigma}} d_{l\bar{\sigma}}, d_{j\sigma}} = \frac{V_{l\vec{k}} \frac{1}{\sqrt{\mathcal{N}}} \phi^*_{\vec{k}}(\vec{R}_l)}{(\varepsilon^+ - \varepsilon_{\vec{k}\sigma})}\tilde{\mathcal{G}}_{d_l n_{d_{l\bar{\sigma}}}, d_{j\sigma}} + \frac{\sum_{\vec{j}\neq l} V_{\vec{j}\vec{k}} \frac{1}{\sqrt{\mathcal{N}}} \phi^*_{\vec{k}}(\vec{R}_{\vec{j}})}{(\varepsilon^+ - \varepsilon_{\vec{k}\sigma})}\langle n_{d_{l\bar{\sigma}}}\rangle \tilde{\mathcal{G}}^{\sigma}_{d_{\vec{j}} d_j}. \quad (65)$$

To close the original setup of Green's functions in Eqs. (50) and (51), we substitute Eq. (65) in Eq. (60) and obtain

$$\left(\varepsilon - \varepsilon_{ld} - U_l + i\Gamma^0_{ll\sigma}\right)\tilde{\mathcal{G}}_{d_{l\sigma} n_{d_{l\bar{\sigma}}}, d_{j\sigma}} = \delta_{lj}\langle n_{d_{l\bar{\sigma}}}\rangle + \langle n_{d_{l\bar{\sigma}}}\rangle \sum_{\tilde{j}\neq l}\left[\Sigma^R_{\tilde{j}l\sigma}(\varepsilon) - i\Gamma_{\tilde{j}l\sigma}\right]\tilde{\mathcal{G}}^{\sigma}_{d_{\tilde{j}} d_j}, \quad (66)$$

where

$$\Gamma^0_{ll\sigma} = \pi \frac{1}{\mathcal{N}} \sum_{\vec{k}} |V_{l\vec{k}}|^2 \delta(\varepsilon - \varepsilon_{\vec{k}\sigma}), \tag{67}$$

which allows us to determine all the necessary Green's functions for the LDOS. Thus, to solve the system composed by Eqs. (50), (51), and (66), we now assume the side-coupled geometry $\vec{R}_l = \vec{R}_j = \vec{0}$ with symmetric couplings $V_{j\vec{k}} = V_{l\vec{k}}$ [see Fig. 1]. By adopting the wideband limit, for the sake of simplicity, from Eqs. (53), (54), and (67), we verify that $\Sigma^R_{jj\sigma} = \Sigma^R_{lj\sigma} = 0$ and $\Gamma_{jj\sigma} = \Gamma_{lj\sigma} = \Gamma^0_{ll\sigma} = \Gamma_\sigma = \Gamma \frac{\rho_{FM\sigma}}{\rho_0}$ depend on the standard Anderson parameter $\Gamma = \pi V^2 \rho_0$ (see Ref. 60 for a precise definition of the wideband limit). We also consider the infinite Coulomb correlation limit ($U_1 = U_2 \to \infty$). A geometry with $\vec{R}_l \neq \vec{R}_j \neq \vec{0}$ and beyond the wideband approximation will be published elsewhere. Thus, the direct Green's function for the impurity $j = 1$ reduces to the form

$$\tilde{\mathcal{G}}^\sigma_{d_1 d_1}(\varepsilon) = \frac{1 - \langle n_{d_1\bar{\sigma}} \rangle}{\varepsilon - \epsilon_{12d\sigma} + i\bar{\Delta}_{12\sigma}}, \tag{68}$$

where

$$\epsilon_{12d\sigma} = \varepsilon_{1d} + \bar{\Sigma}_{12\sigma}(\varepsilon) \tag{69}$$

represents a renormalized energy level dressed by the real part of the nondiagonal self-energy,

$$\bar{\Sigma}_{12\sigma}(\varepsilon) = -(1 - \langle n_{d_1\bar{\sigma}} \rangle)(1 - \langle n_{d_2\bar{\sigma}} \rangle) \frac{(\varepsilon - \varepsilon_{2d})}{(\varepsilon - \varepsilon_{2d})^2 + \Gamma^2_\sigma} \Gamma^2_\sigma, \tag{70}$$

and

$$\bar{\Delta}_{12\sigma} = \Gamma_\sigma - (1 - \langle n_{d_1\bar{\sigma}} \rangle)(1 - \langle n_{d_2\bar{\sigma}} \rangle)\Gamma_\sigma \times \frac{\Gamma^2_\sigma}{(\varepsilon - \varepsilon_{2d})^2 + \Gamma^2_\sigma} \tag{71}$$

is an effective hybridization function. The mixed Green's function $\tilde{\mathcal{G}}^\sigma_{d_2 d_1}(\varepsilon)$ becomes

$$\tilde{\mathcal{G}}^\sigma_{d_2 d_1}(\varepsilon) = -i\Gamma_\sigma \left\{ \frac{1 - \langle n_{d_2\bar{\sigma}} \rangle}{(\varepsilon - \varepsilon_{2d} + i\Gamma_\sigma)} \right\} \tilde{\mathcal{G}}^\sigma_{d_1 d_1}(\varepsilon). \tag{72}$$

Notice that the other Green's functions $\tilde{\mathcal{G}}^\sigma_{d_2 d_2}$ and $\tilde{\mathcal{G}}^\sigma_{d_1 d_2}$ can be derived by swapping $1 \leftrightarrow 2$ in Eqs. (68) and (72).

IV. NUMERICAL RESULTS

A. Numerical parameters

Here, we present the results obtained via the formulation developed in the previous section. The energy scale adopted is the Anderson parameter Γ. We employ the following set of model parameters: $\Gamma = 0.2$ eV, $\varepsilon_{1d} = -10\Gamma$, and $\varepsilon_{2d} = -4.5\Gamma$.[15,21] Such values correspond to a Kondo temperature $T_K \approx 50$ K found in the system Co/Cu(111) with Coulomb interaction $U = 2.9$ eV.[13,15,19] Thus, the Hubbard I approximation is employed with $T = \Gamma/10k_B = 231.1$ K just to avoid Kondo physics. Defining $k_{F\uparrow} = k_F$, we measure the lateral distance R between the STM tip and the impurities in units of k_F^{-1} by introducing the dimensionless parameter $k_F R$ [see Fig. 1]. Finally, in order to generate spin-polarized quantum beats in the LDOS, we substitute Eq. (2) with $P = 0.1$ in Eq. (27).

B. Metallic surface

We begin the analysis in the metallic surface apparatus by dividing our paper into regions we call short, intermediate, and long ranges. The short-range limit presented in Fig. 2(a) reveals that the LDOS, given by Eq. (24) as a function of energy, exhibits two Fano antiresonances. Each one corresponds to the discrete levels of the adatom ($j = 1$) and the subsurface impurity ($j = 2$). The main feature in this situation is that the Fano profile conserves its line shape when the dimensionless parameter $k_F R$ is changed. Additionally, this profile is suppressed for increasing distances, tending to the DOS background of the host.

In Fig. 2(b), we look at how the LDOS evolves with $k_F R$ exactly at the Fano antiresonance $\varepsilon = \varepsilon_{d_1} = -10\Gamma$. At the host site ($k_F R = 0$), the LDOS presents a depletion. Such a dip in the LDOS is a result of charge screening around the impurities by conduction electrons, which suppresses the LDOS of the

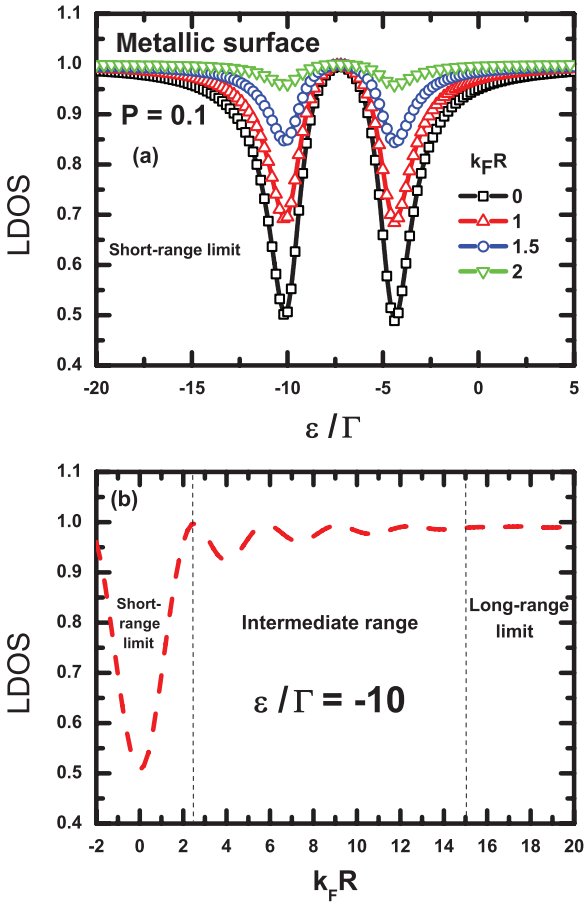

FIG. 2. (Color online) In both panels, we use $k_B T = 0.1\Gamma$. (a) LDOS [Eq. (24)] of a metallic surface with $P = 0.1$ as a function of ε/Γ for different values of $k_F R$ in the short-range limit [see panel (b)]. The Fano profile presents two antiresonances placed at $\varepsilon = \varepsilon_{1d} = -10\Gamma$ and $\varepsilon = \varepsilon_{2d} = -4.5\Gamma$, which display an evanescent behavior for increasing distances. (b) Keeping the energy at $\varepsilon = -10\Gamma$, Friedel oscillations appear in the LDOS.

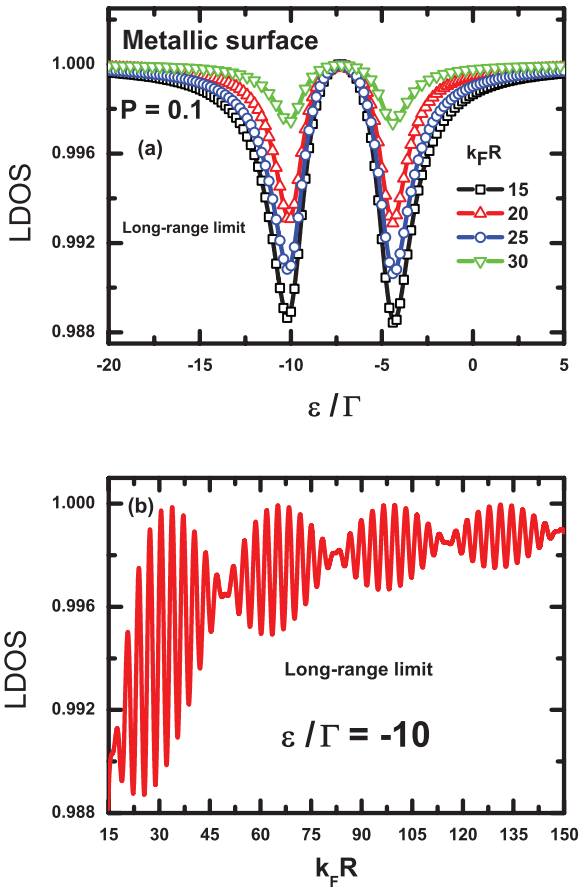

FIG. 3. (Color online) In both panels, we use $k_BT = 0.1\Gamma$. (a) LDOS [Eq. (24)] of a metallic surface with $P = 0.1$ as a function of ε/Γ for different values of k_FR in the long-range limit [see panel (b)]. The Fano profile presents two antiresonances placed at $\varepsilon = \varepsilon_{1d} = -10\Gamma$ and $\varepsilon = \varepsilon_{2d} = -4.5\Gamma$, which display an oscillatory behavior for increasing distances. (b) Damped spin-polarized quantum beats emerge in the LDOS as a function of k_FR with $\varepsilon = \varepsilon_{1d} = -10\Gamma$.

host. Beyond the adatom position, the LDOS is, indeed, dictated by Friedel oscillations, which also lead to a strong decay in the long-range limit [see Fig. 2(b)]. The evanescent feature of the LDOS is a result of the interplay between the Friedel-like expression $A^{2D}_{j\sigma}$ and the Fano parameter $q^{2D}_{j\sigma}$. These quantities are governed by Eqs. (30) and (43) where the former evolves spatially according to the zeroth-order Bessel function J_0. Such damping in the LDOS has already been observed experimentally in a system composed by an Fe host and a Co adatom.[5]

In Fig. 3(a), we plot the Fano line shape in the long-range regime ($k_FR > 15$). The same dips at $\varepsilon = -10\Gamma$ and $\varepsilon = -4.5\Gamma$ are observed as in the short-range limit [Fig. 2(a)]. However, a contrasting feature is found between these two limits. Whereas, in the short-range case, the dips become suppressed as k_FR increases, in both regions of intermediate and long ranges, the dip oscillates with k_FR. This is a result of the oscillatory profile observed in the LDOS for increasing k_FR [see Fig. 2(b)]. In the long-range limit, the oscillations of the dip can be more clearly visualized in Fig. 3(b) where we show the LDOS at $\varepsilon = \varepsilon_{d_1} = -10\Gamma$. A peculiar beating is observed in the LDOS due to the slightly different Fermi wave numbers [see Eq. (27)].

C. Quantum wire

Figure 4(a) shows the LDOS plotted against energy for different k_FR values in the short-range limit. For the STM tip at $k_FR = 0$, the LDOS shows the two-dip structure already observed in Fig. 2(a). In contrast, as k_FR increases, the antiresonances change to resonances, passing through intermediate profiles (asymmetric Fano line shapes). We emphasize that this behavior in the LDOS was recently observed in the experiment performed by Prüser *et al.* with atoms of Fe and Co beneath the Cu(100) surface.[45]

In Fig. 4(b), we observe the evolution of the LDOS with k_FR. Nonevanescent oscillations occur, modulated by an amplitude beating. This undamped behavior is encoded by Eqs. (46) and (49) for Friedel-like oscillations ($A^{1D}_{j\sigma}$) and Fano interference ($q^{1D}_{j\sigma}$), respectively. These quantities are simple trigonometric functions without damping. This feature is due to the absence of an extra dimension for the scattering of the

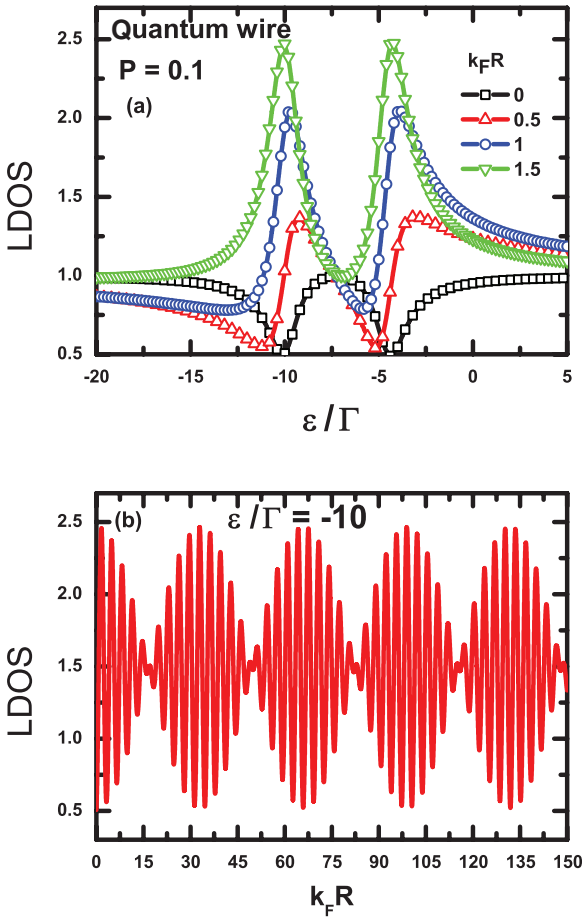

FIG. 4. (Color online) (a) LDOS [Eq. (24)] at $k_BT = 0.1\Gamma$ of a quantum wire with $P = 0.1$ as a function of ε/Γ for different values of positions k_FR. Fano profiles appear around $\varepsilon = \varepsilon_{1d} = -10\Gamma$ and $\varepsilon = \varepsilon_{2d} = -4.5\Gamma$. This pair of antiresonances (black line) can be tuned to resonances (green line) by moving the STM tip laterally. (b) In opposition to the metallic surface device, undamped spin-polarized quantum beats in the LDOS at $\varepsilon = \varepsilon_{1d} = -10\Gamma$ manifest.

electronic wave. On the other hand, in 2D, this propagation is spread in a plane leading to a spatial decay in the LDOS. Thus, the amplitude of the undamped beats is much larger than in the metallic surface device. This means that, in such cases, the LDOS signal can be more easily resolved experimentally.

D. Transport polarization

Another quantity we investigate is the spin polarization given by Eq. (25). As the differential conductance of Eq. (23) is a function of the spin-dependent LDOS $\rho^{\sigma}_{\mathrm{LDOS}}$ of Eq. (21), the ferromagnetic hosts filter electrons that tunnel into (or out of) the STM tip. This filtering is dominated by the majority-spin component. Thus, devices without impurities behave as spin filters with a spatially uniform polarization that coincides with the value given by Eq. (2). Here, we adopt $P = 0.1$. Due to the impurities in the side-coupled geometry and the host dimensionality, this polarization is perturbed in two different forms. In both the metallic surface and the quantum wire as we can see in Figs. 5(a) and 5(b) with applied bias $\phi = \varepsilon_{1d} = -10\Gamma$, the polarization oscillates around $P_T =$ $P = 0.1$. Unlike the metallic surface system where small deviations with damping occur, the electron-focusing effect in the quantum wire leads to undamped and pronounced oscillations. The polarization in the latter case does not exceed $P_T \approx +0.62$ or fall below $P_T \approx -0.5$. Therefore, the polarized current through the junction formed by the STM tip and the surface alternates from spins up (+0.62) to down (−0.5) depending on the tip position. Additionally, along this probing direction, the polarization not only can invert the orientation of the majority-spin component, but also can become zero at some sites where locally, the unbalance of spins is totally suppressed. As a result, we have a tunneling current without polarization in specific positions on the sample surface. On the other hand, as we can see in Fig. 5(a), the amplitude of the beats in the metallic surface polarization is extremely suppressed and does not change its signal ($P_T > 0$). Thus, the quantum wire operates as a spatially resolved spin filter with a higher efficiency.

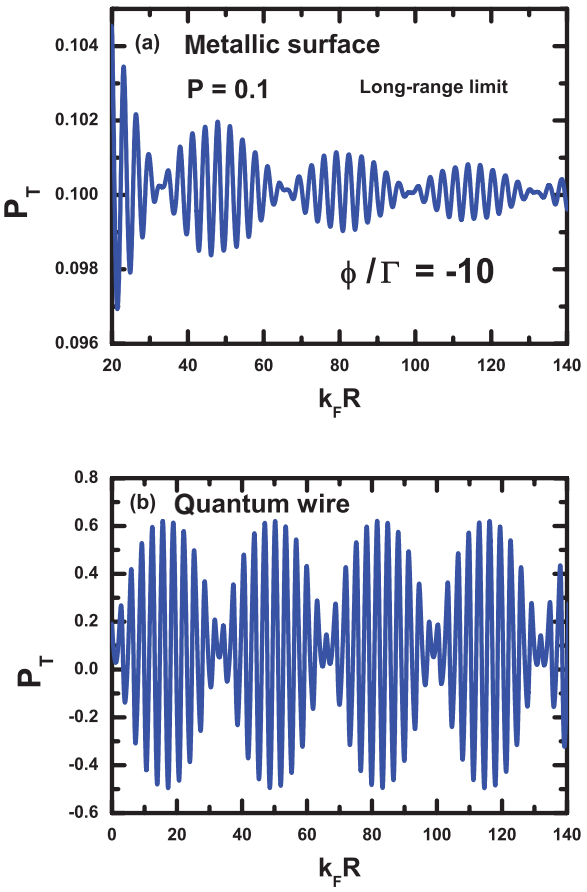

FIG. 5. (Color online) Transport polarization of the ferromagnetic hosts [Eq. (25)] at $k_B T = 0.1\Gamma$ and applied bias $\phi = \varepsilon_{1d} = -10\Gamma$. (a) Damped spin-polarized quantum beats appear in the polarization of the metallic surface device. (b) Undamped types occur in the polarization of the quantum wire. In both situations, we have a spatially resolved spin filter with a polarization that oscillates around $P = 0.1$. In the quantum wire case, this oscillation is more pronounced.

V. CONCLUSIONS

In order to investigate a ferromagnetic system with two impurities, we have calculated the LDOS and the spin polarization of hosts in two different dimensionalities. Impurities in the side-coupled geometry, as outlined in Fig. 1, were taken into account. We analyzed both a metallic surface and a quantum wire described by the two-impurity Anderson model in the picture of a spin-polarized electron gas with impurities away from the Kondo regime. We presented a model in which an unperturbed 1D electron host in the presence of localized states produces undamped behavior in the LDOS Fano profile [see Figs. 4(a) and 4(b)], similar to that observed experimentally.[45] In contrast, our 2D model revealed a damped oscillatory behavior [Figs. 2(a), 2(b), 3(a), and 3(b)]. We demonstrated that these opposed features originated from the interplay between the Friedel-like function and the Fano parameter, which assumed different functional forms according to the host dimensionality. Keeping the energy fixed and tuning the STM tip position, we verified the emergence of spin-polarized quantum beats in the LDOS given by Eq. (24) as well as in the transport polarization of Eq. (25). Such an effect is due to interference between the slightly different Fermi wave numbers $k_{F\uparrow}$ and $k_{F\downarrow}$ [Eq. (27)] in the LDOS, achievable in hosts with low spin polarizations. Therefore, the quantum wire setup behaves as a spatially resolved spin filter with a high efficiency as we can see in Fig. 5(b). Away from the adatom, this device can magnify or can locally invert the original spin orientation of the host, also displaying sites where this polarization is completely quenched. As a possible experimental implementation of this apparatus, we suggest the systems investigated by Prüser.[45] Such setups present the same one-dimensional character as our effective quantum wire model.

ACKNOWLEDGMENTS

This work was supported by the Brazilian agencies CNPq, CAPES, FAPEMIG, and PROPe/UNESP. Support from the PRP/USP within the Research Support Center initiative (NAP Q-NANO) is also acknowledged.

[1] U. Fano, Phys. Rev. **124**, 1866 (1961).
[2] A. E. Miroshnichenko, S. Flach, and Y. S. Kivshar, Rev. Mod. Phys. **82**, 2257 (2010).
[3] A. C. Hewson, *The Kondo Problem to Heavy Fermions* (Cambridge University Press, Cambridge, UK, 1993).
[4] A. C. Seridonio, F. S. Orahcio, F. M. Souza, and M. S. Figueira, Phys. Rev. B **85**, 165109 (2012).
[5] S. L. Kawahara, J. Lagoute, V. Repain, C. Chacon, Y. Girard, J. Klein, and S. Rousset, Phys. Rev. B **82**, 020406R (2010).
[6] A. C. Seridonio, F. M. Souza, and I. A. Shelykh, J. Phys.: Condens. Matter **21**, 095003 (2009).
[7] A. C. Seridonio, F. M. Souza, J. Del Nero, and I. A. Shelykh, Physica E **41**, 1611 (2009).
[8] V. Madhavan, W. Chen, T. Jamneala, M. F. Crommie, and N. S. Wingreen, Science **280**, 567 (1998).
[9] A. Schiller and S. Hershfield, Phys. Rev. B **61**, 9036 (2000).
[10] M. Plihal and J. W. Gadzuk, Phys. Rev. B **63**, 085404 (2001).
[11] H. C. Manoharan, C. P. Lutz, and D. M. Eigler, Nature (London) **403**, 512 (2000).
[12] V. Madhavan, W. Chen, T. Jamneala, M. F. Crommie, and N. S. Wingreen, Phys. Rev. B **64**, 165412 (2001).
[13] N. Knorr, M. A. Schneider, L. Diekhöner, P. Wahl, and K. Kern, Phys. Rev. Lett. **88**, 096804 (2002).
[14] P. Wahl, L. Diekhöner, G. Wittich, L. Vitali, M. A. Schneider, and K. Kern, Phys. Rev. Lett. **95**, 166601 (2005).
[15] C.-Y. Lin, A. H. Castro Neto, and B. A. Jones, Phys. Rev. Lett. **97**, 156102 (2006).
[16] Y.-S. Fu, S.-H. Ji, X. Chen, X.-C. Ma, R. Wu, C.-C. Wang, W.-H. Duan, X.-H. Qiu, B. Sun, P. Zhang, J.-F. Jia, and Q.-K. Xue, Phys. Rev. Lett. **99**, 256601 (2007).
[17] J. M. Aguiar-Hualde, G. Chiappe, E. Louis, and E. V. Anda, Phys. Rev. B **76**, 155427 (2007).
[18] G. Chiappe and E. Louis, Phys. Rev. Lett. **97**, 076806 (2006).
[19] O. Újsághy, J. Kroha, L. Szunyogh, and A. Zawadowski, Phys. Rev. Lett. **85**, 2557 (2000).
[20] A. F. Otte, M. Ternes, K. V. Bergmann, S. Loth, H. Brune, C. P. Lutz, C. F. Hirjibehedin, and A. J. Heinrich, Nat. Phys. **4**, 847 (2008).
[21] M. Ternes, A. J. Heinrich, and W. D. Schneider, J. Phys.: Condens. Matter **21**, 053001 (2009).
[22] J. Figgins and D. K. Morr, Phys. Rev. Lett. **104**, 187202 (2010).
[23] P. Wölfle, Y. Dubi, and A. V. Balatsky, Phys. Rev. Lett. **105**, 246401 (2010).
[24] P. H. Penteado, F. M. Souza, A. C. Seridonio, E. Vernek, and J. C. Egues, Phys. Rev. B **84**, 125439 (2011).
[25] N. Néel, J. Kröger, and R. Berndt, Phys. Rev. B **82**, 233401 (2010).
[26] P. Zhang, Q.-K. Xue, Y. P. Wang, and X. C. Xie, Phys. Rev. Lett. **89**, 286803 (2002).
[27] Y. Qi, J. X. Zhu, S. Zhang, and C. S. Ting, Phys. Rev. B **78**, 045305 (2008).
[28] J. Martinek, M. Sindel, L. Borda, J. Barnaś, J. König, G. Schön, and J. von Delft, Phys. Rev. Lett. **91**, 247202 (2003).
[29] J. Martinek, Y. Utsumi, H. Imamura, J. Barnaś, S. Maekawa, J. König, and G. Schön, Phys. Rev. Lett. **91**, 127203 (2003).
[30] M.-S. Choi, D. Sánchez, and R. López, Phys. Rev. Lett. **92**, 056601 (2004).
[31] J. Martinek, M. Sindel, L. Borda, J. Barnaś, R. Bulla, J. König, G. Schön, S. Maekawa, and J. von Delft, Phys. Rev. B **72**, 121302(R) (2005).
[32] Y. Utsumi, J. Martinek, G. Schön, H. Imamura, and S. Maekawa, Phys. Rev. B **71**, 245116 (2005).
[33] R. Świrkowicz, M. Wilczyński, M. Wawrzyniak, and J. Barnaś, Phys. Rev. B **73**, 193312 (2006).
[34] A. N. Pasupathy, R. C. Bialczak, J. Martinek, J. E. Grose, L. A. K. Donev, P. L. McEuen, and D. C. Ralph, Science **306**, 86 (2004).
[35] M. Sindel, L. Borda, J. Martinek, R. Bulla, J. König, G. Schön, S. Maekawa, and J. von Delft, Phys. Rev. B **76**, 045321 (2007).
[36] K. Hamaya, M. Kitabatake, K. Shibata, M. Jung, M. Kawamura, K. Hirakawa, T. Machida, and T. Taniyama, Appl. Phys. Lett. **91**, 232105 (2007).
[37] K. Hamaya, M. Kitabatake, K. Shibata, M. Jung, M. Kawamura, S. Ishida, T. Taniyama, K. Hirakawa, Y. Arakawa, and T. Machida, Phys. Rev. B **77**, 081302(R) (2008).
[38] M. R. Calvo, J. Fernández-Rossier, J. J. Palacios, D. Jacob, D. Natelson, and C. Untiedt, Nature (London) **458**, 1150 (2009).
[39] J. Hauptmann, J. Paaske, and P. Lindelof, Nat. Phys. **4**, 373 (2008).
[40] I. Weymann and L. Borda, Phys. Rev. B **81**, 115445 (2010).
[41] I. Weymann, Phys. Rev. B **83**, 113306 (2011).
[42] M. Misiorny, I. Weymann, and J. Barnaś, Phys. Rev. Lett. **106**, 126602 (2011).
[43] M. Gaass, A. K. Hüttel, K. Kang, I. Weymann, J. von Delft, and C. Strunk, Phys. Rev. Lett. **107**, 176808 (2011).
[44] M. Misiorny, I. Weymann, and J. Barnaś, Phys. Rev. B **84**, 035445 (2011).
[45] H. Prüser, M. Wenderoth, A. Weismann, and R. G. Ulbrich, Phys. Rev. Lett. **108**, 166604 (2012).
[46] H. Prüser, M. Wenderoth, P. E. Dargel, A. Weismann, R. Peters, T. Pruschke, and R. G. Ulbrich, Nat. Phys. **7**, 203 (2011).
[47] S. Lounis, P. Zahn, A. Weismann, M. Wenderoth, R. G. Ulbrich, I. Mertig, P. H. Dederichs, and S. Blügel, Phys. Rev. B **83**, 035427 (2011).
[48] A. Weismann, M. Wenderoth, S. Lounis, P. Zahn, N. Quaas, R. G. Ulbrich, P. H. Dederichs, and S. Blügel, Science **323**, 1190 (2009).
[49] A. Weismann, Ph.D. thesis, Georg-August-Universität zu Göttingen, 2008.
[50] S. Lounis, Ph.D. thesis, Rheinisch-Westfälische Technische Hochschule (RWTH) Aachen, 2007.
[51] A. Stroppa, X. Duan, M. Peressi, D. Furlanetto, and S. Modesti, Phys. Rev. B **75**, 195335 (2007).
[52] F. M. Souza, Phys. Rev. B **76**, 205315 (2007).
[53] P. Trocha, Phys. Rev. B **82**, 115320 (2010).
[54] P. W. Anderson, Phys. Rev. **124**, 41 (1961).
[55] H. Haug and A. P. Jauho, *Quantum Kinetics in Transport and Optics of Semiconductors*, Springer Series in Solid-State Sciences Vol. 123 (Springer, New York, 1996).
[56] The occupancy of the impurities can strongly depend on the positions of the levels ε_{jd}. In our calculations, we adopt ε_{jd} much smaller than the Fermi level, so the self-consistent calculation yields occupations close to unity (single occupancy).
[57] E. C. Stoner, Proc. R. Soc. London, Ser. A **169**, 339 (1939).
[58] F. M. Souza, J. C. Egues, and A. P. Jauho, Braz. J. Phys. **34**, 565 (2004).
[59] Quantum dot systems may also display a beating pattern, in particular, if one considers two alternate dot levels with slightly different frequencies. In this case, quantum beats appear in the electrical current as a function of time (see Refs. 52 and 53).

[60]The wideband limit consists of (i) neglecting the real part of the tunneling self-energy $\Sigma^R_{lj\sigma}$ (level shift) and (ii) assuming that the linewidths $\Gamma_{lj\sigma}$ are energy-independent constants (see Ref. 55). To summarize, the metallic behavior of the hosts lies in the vicinity of the Fermi level, which ensures the aforementioned assumptions. Thus, we can safely extrapolate to infinity the limits of the integral in Eq. (56) to calculate $\langle n_{d_l\bar{\sigma}} \rangle$ (see Ref. 61).

[61]A. P. Jauho, N. S. Wingreen, and Y. Meir, Phys. Rev. B **50**, 5528 (1994).